Journal of Biomedical Optics

BiomedicalOptics.SPIEDigitalLibrary.org

Use of optical skin phantoms for preclinical evaluation of laser efficiency for skin lesion therapy

Maciej S. Wróbel
Malgorzata Jędrzejewska-Szczerska
Stanislaw Galla
Leszek Piechowski
Miroslaw Sawczak
Alexey P. Popov
Alexander V. Bykov
Valery V. Tuchin
Adam Cenian

SPIE.

Use of optical skin phantoms for preclinical evaluation of laser efficiency for skin lesion therapy

Maciej S. Wróbel,[a,*] Malgorzata Jędrzejewska-Szczerska,[a] Stanislaw Galla,[a] Leszek Piechowski,[b] Miroslaw Sawczak,[b] Alexey P. Popov,[c,d] Alexander V. Bykov,[c,d] Valery V. Tuchin,[c,d,e,f] and Adam Cenian[b]

[a]Gdańsk University of Technology, Faculty of Electronics, Telecommunications and Informatics, Department of Metrology and Optoelectronics, Narutowicza 11/12, Gdańsk 80-233, Poland
[b]Polish Academy of Sciences, The Szewalski Institute of Fluid-flow Machinery, Physical Aspects of Ecoenergy Department, Fiszera 14, Gdańsk 80-952, Poland
[c]University of Oulu, Faculty of Information Technology and Electrical Engineering, Optoelectronics and Measurement Techniques Laboratory, P.O. Box 4500, FI-90014 Oulu, Finland
[d]Tomsk State University, 36 Lenina Avenue, Tomsk 634050, Russia
[e]Saratov State University, Research-Educational Institute of Optics and Biophotonics, 83 Astrakhanskaya, Saratov 410012, Russia
[f]Russian Academy of Sciences, Institute of Precise Mechanics and Control, 24 Rabochaya, Saratov 410028, Russia

Abstract. Skin lesions are commonly treated using laser heating. However, the introduction of new devices into clinical practice requires evaluation of their performance. This study presents the application of optical phantoms for assessment of a newly developed 975-nm pulsed diode laser system for dermatological purposes. Such phantoms closely mimic the absorption and scattering of real human skin (although not precisely in relation to thermal conductivity and capacitance); thus, they can be used as substitutes for human skin for approximate evaluation of laser heating efficiency in an almost real environment. Thermographic imaging was applied to measure the spatial and temporal temperature distributions on the surface of laser-irradiated phantoms. The study yielded results of heating with regard to phantom thickness and absorption, as well as laser settings. The methodology developed can be used in practice for preclinical evaluations of laser treatment for dermatology. [DOI: 10.1117/1.JBO.20.8.085003]

Keywords: tissue-mimicking phantoms; optical properties; lasers in medicine; thermography; tissues.

Paper 150155PRR received Mar. 13, 2015; accepted for publication Jul. 1, 2015; published online Aug. 11, 2015.

1 Introduction

Optical skin phantoms are materials which mimic optical properties (reduced scattering coefficient μ_s', absorption coefficient, μ_a), of human tissues.[1,2] Phantoms have known and controlled properties, which enable them to be used as calibration standards for testing and development of optical noninvasive diagnostic methods.[3–7] In the case of laser therapy, new devices require assessment of their therapeutic efficiency before they can be introduced into clinical practice. Such tests are commonly conducted on *ex vivo* tissues or on animals *in vivo*. Since the distribution of light in phantoms is identical to that of real tissues, we propose using optical phantoms simulating skin optical properties as an equivalent for real human skin.[8–10] Such phantoms are made of polyvinyl chloride plastisol (PVCP) as a matrix material and zinc oxide (ZnO) nanoparticles as scattering agents. However, it must be mentioned that the thermal properties of phantoms differ a bit from those of real skin: the value of skin thermal conductivity—for human epidermis, 0.209 $\mathrm{W\,m^{-1}\,K^{-1}}$; dermis, 0.293–0.322 $\mathrm{W\,m^{-1}\,K^{-1}}$ (see Ref. 11 and its details) is slightly higher than that of PVCP ranges, which is from 0.14 to 0.28 $\mathrm{W\,m^{-1}\,K^{-1}}$, both at 298 K; and for thermal capacitance, the skin averages about 3200 $\mathrm{J\,kg^{-1}\,K^{-1}}$, while the PVCP ranges from 1200 to 2000 $\mathrm{J\,kg^{-1}\,K^{-1}}$, at 298 K; data from the literature.[10–15] Therefore, it is expected that the skin temperature in reality will be lower than that measured for proposed phantoms; yet, the difference should decline when considering short laser pulses, as the role of thermal conductivity decreases. In the proposed medical application of a laser, when the energy is delivered to a targeted diseased tissue in a time shorter than the tissue thermal relaxation time,[16,17] it is most important to investigate the maximal temperature which the tissue can achieve. This depends on the volume density of energy absorbed by the tissue, as well as its thermal capacity. Temperature rise is proportional to the density of absorbed energy and inversely proportional to the thermal capacity of tissue. Thus, the differences in temperature between phantoms and real skin can be recalculated accounting for differences in their thermal properties. It is also known that the heat transport in the skin is facilitated by blood flow.[18–20] The related heat convection by blood decreases temperature in the real skin if compared with phantom, which allows for more safety when applying the results of phantom investigations to a medical-therapy planning. The problem of heat convection by blood vessel has not been investigated in this paper and should be dealt with in future works.

For a very short time after the irradiation, temperature rise is inversely proportional to the heat capacity of the irradiated skin. Yet, for longer times after irradiation, the heat conductivity of the tissue layers beneath the skin, such as fat, muscle, and bones, also affects the temperature distributions. However, in this

*Address all correspondence to: Maciej S. Wróbel, E-mail: maciejswrobel@gmail.com

1083-3668/2015/$25.00 © 2015 SPIE

paper, we are focused mostly on the skin thermal response after the irradiation, when the tissue temperature is the highest. Thus, the tissues lying under the skin would have no noticeable effects on our measurements because they are relevant only for the cooling rate, which happens over much longer time scales.

In this paper, we tested the phantoms with our previously developed pulsed diode laser system with a 975-nm central wavelength. This laser is intended to achieve deep penetration into tissue, similar to that of common Nd:YAG lasers. Its advantages are a much smaller cost and it is lightweight, which increases the availability of devices based on pulsed diode lasers on the market. The expected area of application of the aforementioned diode laser is treatment of hemangiomas and neurofibroma (Recklinghausen disease).[17,21] The tests were conducted with various laser settings to choose an optimal set of parameters for pulsed photothermolysis therapy of skin lesions with minimal damage to the tissues surrounding the target area. Irradiated phantoms' thermal effects were registered using an infrared (IR) camera in the 8 to 14 μm range. Temperature spatial distributions and time profiles were recorded for phantoms with and without introduced absorption and varied thickness, while containing the same scattering (identical to μ_s' of human skin). The motivation behind creating a phantom with low (almost none) absorption was to create a "basic" scattering phantom, which could then be suited for a required skin phototype by adding a specific concentration of absorbers, such as was done in this paper, with the focus on skin phototype I. Moreover, testing the scattering nonabsorbing phantom allowed us to check optical and thermal radiation distributions when incident light is not absorbed and only scattering (which is roughly the same for all phototypes) governs the photon migration paths. The surface temperatures of phantoms were measured from both sides: on the irradiated side as well as the backside to determine penetration of the laser radiation into the phantom.

2 Materials

2.1 *Optical Phantoms*

The phantoms possess optical parameters (absorption coefficient μ_a and reduced scattering coefficient μ_s') close to the parameters of real human skin in the near-IR wavelength range. We have developed and characterized three types of optical skin phantoms. All phantoms had roughly the same scattering coefficient, similar to that of typical human skin. The phantoms were produced according to our previously developed procedures[22,23] and consist of a PVCP as a matrix material, which gives the phantom its shape and mechanical properties. The scattering nanoparticles of ZnO are used to simulate the μ_s' of real human skin by precise determination of the required concentration and sizes. The third element is a black ink, which is a broadband absorbing agent. The nanoparticles and ink are mixed in a solution, then sonicated to destroy particle clusters and poured into molds of the required shape. After degassing, the mixture is heated to about 180°C for 1 h. The PVCP polymerizes and becomes transparent itself, concluding the phantom fabrication process. Then the phantom parameters (μ_a and μ_s') are retrieved by an inverse adding-doubling method from photometric measurements.[23,24] Total reflectance and total transmission are measured with a spectrophotometric system[25] with integrating spheres (OL-750, Optronic Laboratories), while the sample thickness and refractive indices[26] are measured by optical coherence tomography (Hyperion OCT System, Thorlabs) and the Abbe refractometer (Atago, Japan), respectively.

The μ_s' of prepared skin phantoms at the target wavelength of 975 nm is, as shown in Fig. 1(a), in the range of 2.09 to 2.69 mm^{-1}, which is a close match to the optical properties found in literature compilations of optical properties of tissues,[9,27] which are in the range of 2.1 to 3.3 mm^{-1} for epidermis, with slightly lower values for deeper tissues, such as dermis 1 to 3 mm^{-1} and subcutaneous adipose tissue 1 to 1.8 mm^{-1}. Thus, we believe that our values are a good match to literature data, especially considering the fact that our phantoms are relatively thick and homogeneous and as such are an averaged substitute of skin as a whole. The absorption properties are, in general, more variable in the human population, so μ_a about 0.2 mm^{-1} is also in the normal range for human skin. Based upon the measurements, we conclude that the phantoms' optical properties, μ_a and μ_s', successfully mimic the optical properties of typical human skin at the required wavelength.[22,23] The parameters and their dependence on the wavelength in the 600 to 1100 nm range are presented in Fig. 1. The increment of μ_s' for the wavelength was fitted using an expression $\mu_s' = a\lambda^{-h}$, with λ in nm and μ_s' in mm^{-1}. The resulting values of h are in

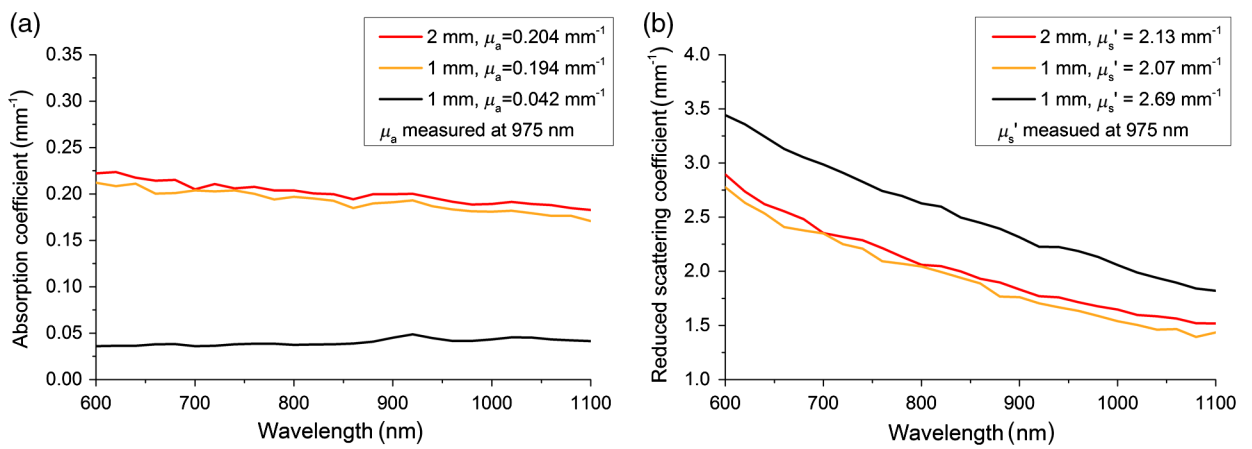

Fig. 1 (a) Measured absorption coefficient and (b) reduced scattering coefficient of produced phantoms used in this study. The properties of each phantom type for a specified wavelength (same as that of a laser) are shown in the legend.

the range of 1.035 to 1.093 for all phantoms, while parameter "a" is between 2276 and 2990, with fit parameters $r^2 = 0.99$ and $\chi^2 < 0.0001$, which indicates a good fit. This confirms that the reduced scattering coefficient in all phantoms follows a roughly identical and expected wavelength dependence.[10,27]

2.2 *Laser System*

A previously developed high-power pulsed diode laser radiating at 975 nm was used for this study.[28] The laser control system enables the setting of the following parameters of a laser pulse: a pulse length (τ, from 2 μs to ~66 ms with stepwise increments $\Delta\tau = 2$ μs), a pulse period (T, from 50 to 500 ms with stepwise increments $\Delta T = 10$ ms), and a pulse-peak power from 0 to 20 W. The laser diode is coupled to an optical fiber with a 600-μm core diameter. The laser radiation is emitted from a bare fiber enclosed in a protective pen-shaped holder for easy manipulation by the clinicians. We use a standard fiber certified for medical applications. The laser exhibits a Gaussian beam intensity profile in the transverse direction.

3 Methods

3.1 *Thermal Effects of Laser Irradiation of Skin Phantoms*

To investigate the efficiency of a laser system for photothermal therapy, we have conducted an experiment, simulating real laser–tissue interactions and tissue thermal response. Optical skin phantoms were treated by pulsed laser radiation. Subsequent thermographic imaging[29–34] of the irradiated area was used to measure the temporal profiles during and after the irradiation. The laser-pulse parameters were varied to determine the optimal values for tissue irradiation which would provide best results of therapy.

Three types of phantoms were used, all with roughly the same scattering coefficients. Two phantoms with a thickness of 1 and 2 mm were denoted "absorbing" because their μ_a matched that of the tissue. The other phantom with very low absorption ($\mu_a = 0.04$ mm^{-1}), exhibiting only intrinsic absorption of the material was called the "nonabsorbing" phantom. This phantom was also 1-mm thick. Use of such phantoms permitted the investigation of heating effects related to the presence of absorption in a sample, as well as determination of the amount of heat transmitted through the sample with different thicknesses. The chosen thickness is a clinically relevant example of an average depth of the pathological features of human skin[35] and assessment of these two depths gives the fastest and most valuable results. The skin phantoms were created to have a rather large thickness and overall area as an approximation of a two-dimensional slab with infinite thickness, in order to achieve a natural optical and thermal radiation diffusion process, as would normally happen in real skin. A smaller thickness would result in unpredicted optical and thermal radiation distribution dude to the boundary conditions at the backside of the phantom. This is the case regardless of phantom thickness, but becomes negligible with greater thickness. Thus, the actual optical and thermal radiation distributions on the front side are a very good approximation of the real situation. According to the best of the authors' knowledge, our approach is the best possible approximate solution to this problem.

The experimental set-up is presented in Fig. 2 and consists of a pulsed diode laser with a therapeutic head directly facing the phantom from a distance of 30 mm, an optical skin phantom mounted in the center, and two configurations of an IR camera (VIGOcam v5, VIGO System S.A., Poland) with microbolometer measuring at an 8- to 14-μm wavelength.[36,37] The camera was calibrated prior to use with a supplied manufacturer black body radiation source with a calibrated temperature sensor. It was situated at 45 deg angle and at a 4-mm distance from the phantom area, facing either the phantom from the laser side (front side), to measure the temperature at the phantom surface, or from the other side (backside), for determination of the radiation passing through the bulk of the phantom.

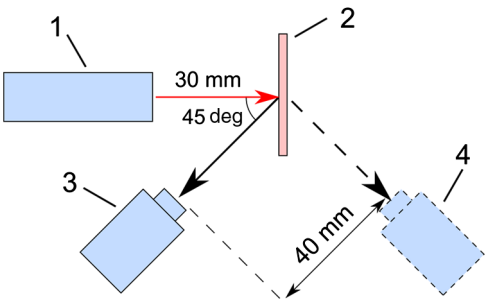

Fig. 2 Scheme of the measurement setup, consisting of: (1) a diode laser, (2) an optical skin phantom, (3) an infrared camera situated at "front" side, and (4) "backside" position. Distances between the elements of the set-up are shown. The red line denotes the laser beam at 975 nm, while the black lines represent the thermal radiation measured at 8 to 14 μm wavelength.

The camera recorded images with a resolution of 384×288 pixels, which corresponds to a 22×15 mm^2 area of a phantom, with a speed of 20 frames/s. The image recording started prior to the laser irradiation, to measure the initial temperature of the phantom. It continued during the laser irradiation, and shortly after ceasing the irradiation. Thus, the whole process of heating from the initial state and part of the cooling process was measured. After each measurement, the phantoms were allowed to cool down back to the initial temperature before starting another irradiation measurement.

4 Results

The thermal response of phantoms was measured for different laser-pulse parameters, including pulse width τ, pulse period T, laser peak power P, and number of pulses N. The images were recorded from the surface of a 1-mm thick absorbing phantom, and the results are presented in Fig. 3(a). The laser power was set at $P = 10$ W and period $T = 50$ ms. The temperature increases with the number of pulses N, from 0 to 80, as well as with the length of the pulse τ, from 15 to 25 ms. Measurements presented in Fig. 3(b) were carried out on various phantoms at set laser parameters: $T = 50$ ms, $\tau = 25$ ms, $P = 10$ W. For absorbing ($\mu_a \sim 0.2$ mm^{-1}) phantoms with different thicknesses (1 and 2 mm), the temperature has risen by about 25°C in both cases. There is no significant change in temperature maximum achieved regardless of the thickness (measured at front)—compare Figs. 4 and 5. The phantoms without introduced absorption ($\mu_a = 0.04$ mm^{-1}) exhibit almost no thermal response, with <1°C maximum increase in temperature—see Fig. 6.

Temporal evolution of temperature measured at the center of the laser spot (maximum temperature) was measured before, during, and shortly after laser irradiation of phantoms for laser parameters ($T = 50$ ms, $\tau = 25$ ms, $P = 10$ W, and applied number of pulses $N = 60$).

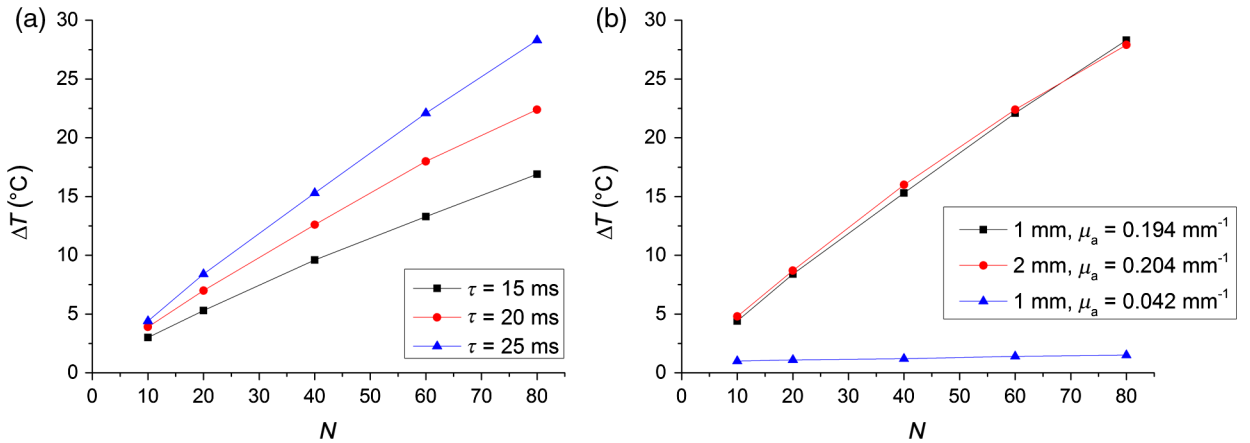

Fig. 3 Temperature increase as a function of the number of pulses N, at constant peak $P = 10$ W and $T = 50$ ms, (a) for different pulse widths τ for 1-mm thick absorbing ($\mu_a = 0.194$ mm^{-1}) phantom and (b) for different phantom thickness (frontal measurement) for pulse width $\tau = 25$ ms (b).

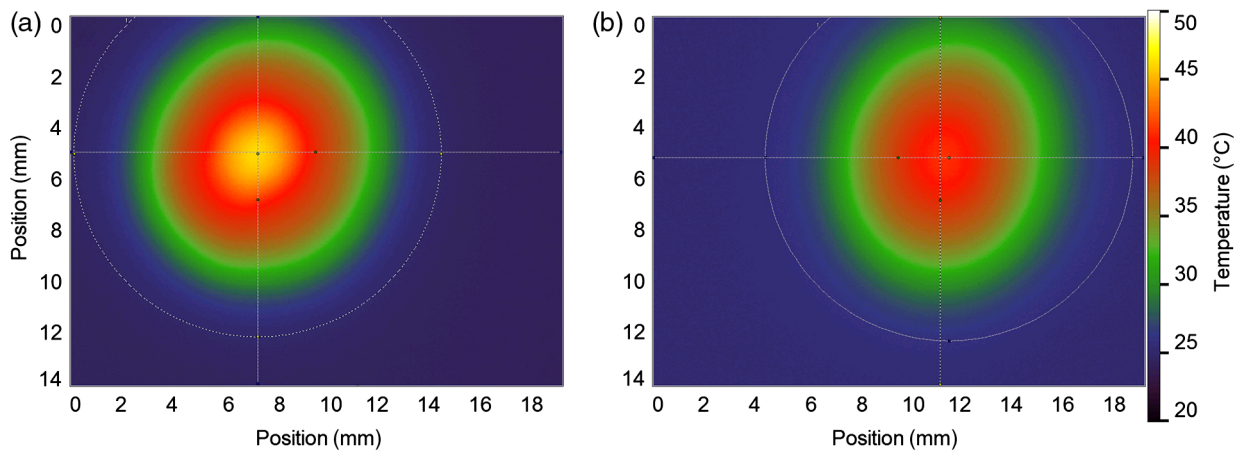

Fig. 4 Measured spatial temperature distribution on the front (a) and back (b) surfaces of 1-mm thick absorbing phantom; laser parameters: $T = 50$ ms, $\tau = 25$ ms, $N = 60$, diameter of incident beam is ~10 mm.

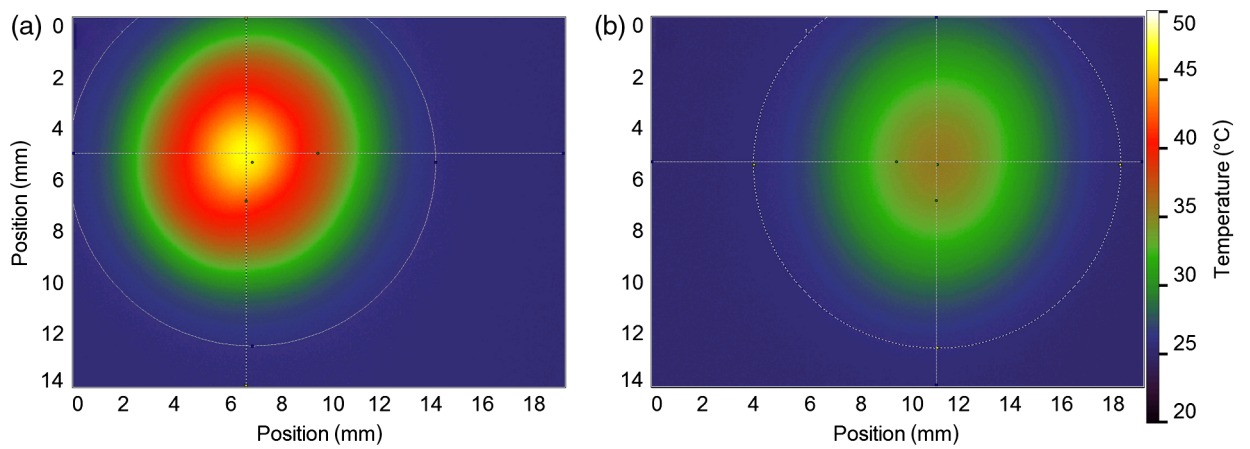

Fig. 5 Measured spatial temperature distribution on the front (a) and back (b) surfaces of 2-mm thick absorbing phantom; laser parameters: $T = 50$ ms, $\tau = 25$ ms, $N = 60$, diameter of incident beam is ~10 mm.

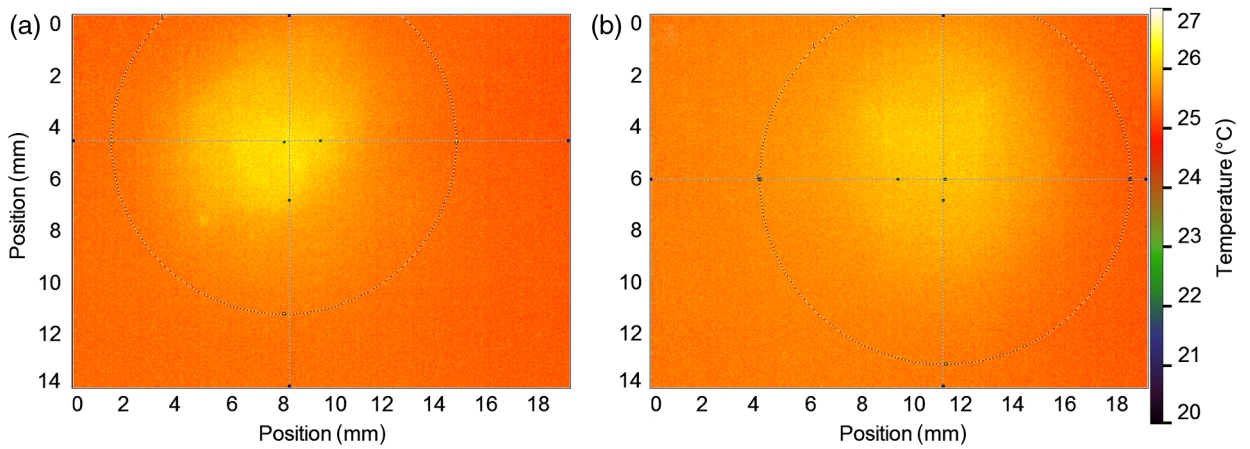

Fig. 6 Measured spatial temperature distribution on *nonabsorbing* 1-mm thick phantom from front (a) and backside (b); laser parameters: $T = 50$ ms, $\tau = 25$ ms, $N = 60$, diameter of incident beam is ~10 mm.

The temporal profiles of temperature for front and backside configuration of the camera for all considered phantoms are presented in Fig. 7(a). Regardless of thickness (1 or 2 mm), the same peak temperature is achieved at the front surface of the phantoms. However, the thicker phantom exhibited a faster rise of temperature and reached the maximum about 1 s earlier than the thinner one. After the laser irradiation ceases, the heat initially dissipates at a faster rate for the thicker phantom, but the process decelerates and the temperatures for both phantoms converge roughly after 15 s. The measurements related to backside imaging show significantly smaller maximal temperatures for phantoms with greater thickness. A difference of 1 mm in thickness corresponds to a drop of temperature of about 7°C at the end of laser irradiation.

For thin phantoms, the cooling process observed from front and backside proceeds at similar rates. A slightly slower temperature decline on the back side is related to additional heat influx from the hotter front side of the phantom. As the temperatures of the front and back sides reach a similar level, further energy dissipation from the irradiated to other cooler regions (and air) on both sides is similar, as are their temperature temporal evolutions (cooling rate). However, thicker phantoms exhibit significantly different characteristics. First, the temperature in the front side of the 2 mm phantom shows initially faster and later slower energy dissipation from the irradiated region than in the case of the thinner (1 mm) phantom. The initial faster dissipation may be possibly related to the larger heat capacitance of the thicker material. In the case of back side temperature, its evolution is almost frozen during the first 7 s after laser irradiation was turned-off, i.e., the thermal influx from the hotter side balances the flux of dissipated energy. It should be added that the maximum temperature on the back side of thicker phantoms is much lower than that of thinner phantoms (less photons reach the back side of thicker phantoms)—this decreases the dissipated energy flux, which is related to temperature gradient.

Spatial profiles of temperatures at the front and back sides for various phantoms are presented in Fig. 7(b). The profiles are taken along the Y-axis as presented in Figs. 4–6, i.e., they include maximum temperature of the distributions. The central part of the distribution presents a character close to normal distribution, with side wings evident mainly for the front side measurements. This central part represents the irradiation region

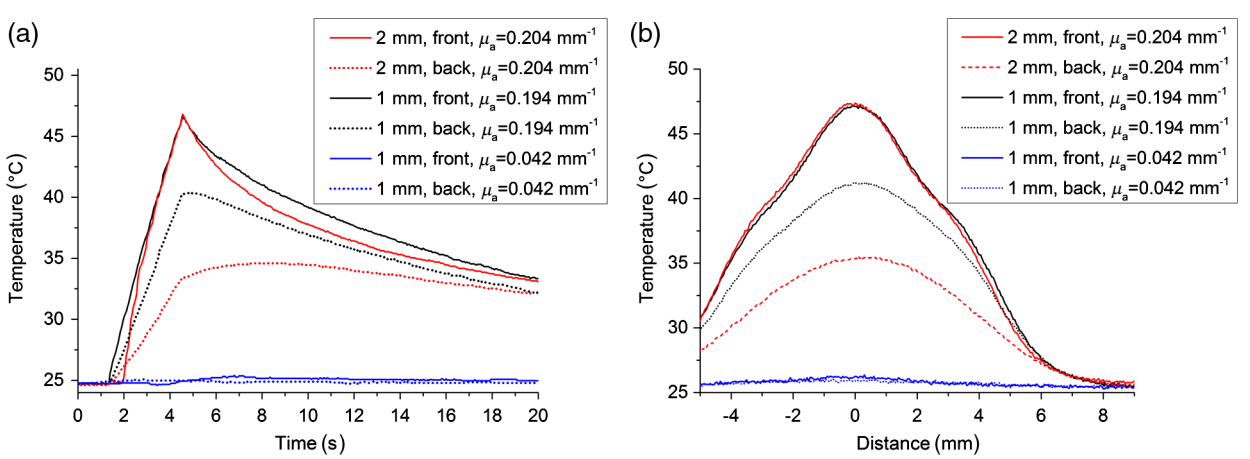

Fig. 7 (a) Temporal profiles for different phantoms, measured from front and backside and (b) spatial temperature profiles along Y-axis from Figs. 4 to 6 crossing temperature maximum, at the end of laser irradiation, after ~3 s of exposure. Measurements were conducted using laser parameters: $T = 50$ ms, $\tau = 25$ ms, $N = 60$.

where the diameter of Gaussian distribution is equal to 10 mm. The side lobes are due to heat dissipation processes induced by thermal conductivity. The side lobes in the case of back side images can still be seen for thinner (1 mm) phantoms. For thicker (2 mm) phantoms, the effect disappears. This behavior can be explained, assuming a very small radiation flux (as is absorbed in front layers) in the case of the 2-mm phantom, so the main feature of profile is determined by thermal diffusivity from hotter regions. This means that in the case of studied radiation (at 975-nm wavelength), the possible localization of laser-illuminated area within tissue layers <2 mm depth (practically 0.5 absorption length) is limited. Both the temperature distributions in phantoms as well as irradiating laser beam intensity in a transverse direction have a Gaussian profile. This, therefore, proves that for short laser pulses, a volumetric rise in temperature is proportional to the introduced energy. This is true also for shallow tissues near the surface, which was measured by a front side measurement. Since the heat capacity of the phantom is roughly three times smaller than the heat capacity of the skin, then knowing the temperature rise in a phantom, and following a simple equation, it is possible to calculate an approximate temperature rise for the skin, assuming the same irradiation.

5 Conclusion

We have used optical skin phantoms, as a substitute for real human skin, for preclinical evaluation of a 975-nm pulsed diode laser. Optical phantoms are a reliable substitute for *ex vivo* tissues because of their stable, known, and controlled properties, which reproduce absorption and scattering coefficients of a real human skin. Spatial and temporal temperature distributions were recorded by an IR camera during and after laser irradiation of the phantom surface. Different laser parameters, such as duration and number of the pulses, were used to evaluate their heating efficiency. Measurements were carried out from the front as well as the back of the phantoms in relation to laser irradiation, to measure the changes in heating efficiency for deeper layers. The influence of absorption coefficient of phantoms was also studied. The results show a huge dependency on the absorption coefficient, with <1°C rise in temperature for a nonabsorbing phantom. Backside measurements yielded a reduction in achieved peak temperature by about 7°C for 1 mm and by 12°C for 2-mm thick phantoms, while preserving the Gaussian profile of temperature distribution.

Results of this study allow for quantifying the heating efficiency of laser radiation with regards to the laser settings and phantom properties. The phantom absorption coefficient and change in thickness were modified to assess its usefulness for deeper skin diseases. We have shown that the use of phantoms as substitutes of human skin with subsequent thermographic imaging can be successively used for evaluation of new lasers for dermatological purposes. This study served as a preclinical test prior to the clinical trials conducted by a dermatologist for treatment of skin diseases, such as hemangiomas and neurofibroma, or to provide tumor cell thermally induced apoptosis. Results of the presented investigations were helpful in the determination of laser power range for medical therapy of hemangiomas and neurofibroma performed by Szymańczyk, a dermatologist from Warsaw Medical University in June 2014 (data are going to be published). It must be underlined that the maximum temperature achieved in the real-skin treatment is smaller than that in phantom experiments (due to higher heat conductivity and possible heat convection by blood), which increases therapy safety.

Acknowledgments

This study was partially supported by the National Science Center, Poland, under the Grant 2011/03/D/ST7/03540; DS Programs of the Faculty of Electronics, Telecommunications and Informatics, Gdańsk University of Technology; European Cooperation in Science and Technology (COST) Action BM1205; Russian Presidential Grant NSh-703.2014.2; and the Government of the Russian Federation Grant 14.Z50.31.0004. The authors L.P. and A.C. acknowledge the financial support from the National Science Centre (NCN—Poland), project No. 2914/B/T02/2011/40.

References

1. B. W. Pogue and M. S. Patterson, "Review of tissue simulating phantoms for optical spectroscopy, imaging and dosimetry," *J. Biomed. Opt.* **11**(4), 041102 (2006).
2. V. V. Tuchin, "Light scattering study of tissues," *Phys.-Uspekhi* **40**(5), 495 (1997).
3. J. Pluciński and A. F. Frydrychowski, "New aspects in assessment of changes in width of subarachnoid space with near-infrared transillumination/backscattering sounding, part 1: Monte Carlo numerical modeling," *J. Biomed. Opt.* **12**(4), 044015 (2007).
4. R. L. Barbour et al., "Validation of near infrared spectroscopic (NIRS) imaging using programmable phantoms," *Proc. SPIE* **6870**, 687002 (2008).
5. T. Myllylä et al., "Optical sensing of a pulsating liquid in a brain-mimicking phantom," *Proc. SPIE* **8799**, 87990X (2013).
6. M. Ali Ansari, S. Alikhani, and E. Mohajerani, "A hybrid imaging method based on diffuse optical tomography and optomechanical method to detect a tumor in the biological phantom," *Opt. Commun.* **342**, 12–19 (2015).
7. C. Böcklin et al., "Mixing formula for tissue-mimicking silicone phantoms in the near infrared," *J. Phys. Appl. Phys.* **48**(10), 105402 (2015).
8. R. B. Saager et al., "Multilayer silicone phantoms for the evaluation of quantitative optical techniques in skin imaging," *Proc. SPIE* **7567**, 756706 (2010).
9. A. N. Bashkatov, E. A. Genina, and V. V. Tuchin, "Optical properties of skin, subcutaneous, and muscle tissues: a review," *J. Innov. Opt. Health Sci.* **4**(1), 9–38 (2011).
10. V. V. Tuchin, *Tissue Optics: Light Scattering Methods and Instruments for Medical Diagnosis*, SPIE Press, Bellingham, WA (2007).
11. M. L. Cohen, "Measurement of the thermal properties of human skin: a review," *J. Invest. Dermatol.* **69**(3), 333–338 (1977).
12. P. A. Hasgall et al., "ITIS database for thermal and electromagnetic parameters of biological tissues," Version 2.5, http://www.itis.ethz.ch/database (1 August 2014).
13. K. R. Holmes, "Thermal Properties," http://users.ece.utexas.edu/~valvano/research/Thermal.pdf
14. S. Patrick, *Practical Guide to Polyvinyl Chloride*, iSmithers Rapra Publishing, Shrewsbury, UK (2005).
15. W. V. Titow, *PVC Technology*, 4th ed., Elsevier Applied Science Publishers, London (1984).
16. C. C. Dierickx et al., "Thermal relaxation of port-wine stain vessels probed in vivo: the need for 1-10-millisecond laser pulse treatment," *J. Invest. Dermatol.* **105**(5), 709–714 (1995).
17. G. Shafirstein et al., "Mathematical modeling of selective photothermolysis to aid the treatment of vascular malformations and hemangioma with pulsed dye laser," *Lasers Med. Sci.* **22**(2), 111–118 (2007).
18. H. Arkin, L. X. Xu, and K. R. Holmes, "Recent developments in modeling heat transfer in blood perfused tissues," *IEEE Trans. Biomed. Eng.* **41**(2), 97–107 (1994).
19. A. Nowakowski, "Quantitative active dynamic thermal IR-imaging and thermal tomography in medical diagnostics," in *Medical Devices and*

Systems, p. 22, Taylor & Francis Group LLC, CRC Press, Boca Raton, Florida (2006).
20. V. De Santis and M. Feliziani, "EMF exposure: a numerical model to predict the temperature increase in biological vascularized tissues," in *14th Conf. on Microwave Techniques*, pp. 1–4 (2008).
21. J. Szymańczyk, "'Laseroterapia—zastosowanie w dermatologii,' (Laser therapy–dermatological applications) [in Polish]," *Dermatologia* **3**(3), 12 (1998).
22. M. S. Wróbel et al., "Multi-layered tissue head phantoms for noninvasive optical diagnostics," *J. Innov. Opt. Health Sci.* **08**(3), 1541005 (2015).
23. M. S. Wróbel et al., "Measurements of fundamental properties of homogeneous tissue phantoms," *J. Biomed. Opt.* **20**(4), 045004 (2015).
24. S. A. Prahl, M. J. van Gemert, and A. J. Welch, "Determining the optical properties of turbid media by using the adding–doubling method," *Appl. Opt.* **32**(4), 559–568 (1993).
25. R. Z. Morawski, "Measurement data processing in spectrophotometric analysers of food," *Metrol. Meas. Syst.* **19**(4), 623–652 (2012).
26. K. Karpienko, M. S. Wróbel, and M. Jędrzejewska-Szczerska, "Determination of refractive index dispersion using fiber-optic low-coherence Fabry–Perot interferometer: implementation and validation," *Opt. Eng.* **53**(7), 077103 (2014).
27. S. L. Jacques, "Optical properties of biological tissues: a review," *Phys. Med. Biol.* **58**(11), R37–R61 (2013).
28. L. Piechowski et al., "Pulsed dermatologic 20 W diode-laser emitting at 975-nm," *Proc. SPIE* **8703**, 870304 (2013).
29. A. Mazikowski, R. Hypszer, and M. Jedrzejewska-Szczerska, "Modeling of noncontact temperature measurement system using multiwavelength pyrometry," *Proc. SPIE* **4516**, 120–124 (2001).
30. M. Jędrzejewska-Szczerska et al., "Investigation of photothermolysis therapy of human skin diseases using optical phantoms," *Proc. SPIE* **9447**, 944715 (2015).
31. J. Ruminski et al., "Thermal parametric imaging in the evaluation of skin burn depth," *IEEE Trans. Biomed. Eng.* **54**(2), 303–312 (2007).
32. J. Rizkalla et al., "Computer simulation/practical models for human thyroid thermographic imaging," *J. Biomed. Sci. Eng.* **08**(04), 246–256 (2015).
33. N. Maniar et al., "The effect of using different regions of interest on local and mean skin temperature," *J. Therm. Biol.* **49–50**, 33–38 (2015).
34. S. Wu, W. Lin, and S. Xie, "Skin heat transfer model of facial thermograms and its application in face recognition," *Pattern Recognit.* **41**(8), 2718–2729 (2008).
35. C. M. Balch et al., "Final Version of 2009 AJCC melanoma staging and classification," *J. Clin. Oncol.* **27**(36), 6199–6206 (2009).
36. S. Galla and A. Konczakowska, "Application of infrared thermography to non-contact testing of varistors," *Metrol. Meas. Syst.* **20**(4), 677–688 (2013).
37. A. Rogalski and K. Chrzanowski, "Infrared devices and techniques (revision)," *Metrol. Meas. Syst.* **21**(4), 565–618 (2014).

Maciej S. Wróbel received his BSc and MSc in electronics and telecommunication, specialty: optoelectronics, from Gdańsk University of Technology in 2012 and 2013, respectively. He is currently a PhD student at the same university. His main research area is biophotonics, and he focuses on spectroscopic methods of biological tissue analysis, tissue-mimicking phantoms for noninvasive optical sensing, signal processing, and fiber-optic sensors.

Malgorzata Jędrzejewska-Szczerska received her PhD degree with honors in electronics from the Gdańsk University of Technology in 2008. Currently, she is an assistant professor in the Department of Metrology and Optoelectronics. Her main research area is biophotonics and she focuses on use of low-coherence interferometry, fiber-optic technology, and application of optical measurements in biomedicine.

Stanislaw Galla is an assistant professor in the Department of Metrology and Optoelectronics, Faculty of Electronics, Telecommunication and Informatics, Gdańsk University of Technology. His main research interest is nondestructive testing using thermal imaging, and electromagnetic compatibility testing.

Leszek Piechowski is a main specialist in the Physical Aspects of Ecoenergy Department in the Szewalski Institute of Fluid-Flow Machinery (IFFM), Polish Academy of Sciences in Gdańsk. He specializes in laser technologies, measurement techniques including plasma diagnostics and control systems.

Miroslaw Sawczak is an assistant professor in the Department of Photophysics of IFFM PASci in Gdansk. In 2003, he defended his PhD dissertation on the diagnostics and optimization of the high-power CO_2 laser radiation. He is an expert in nondestructive spectroscopic techniques for material analysis and has extensive experience in the designing and development of the analytical equipment using lasers and x-ray radiation.

Alexey P. Popov graduated from the Physics Department of Moscow State University (Russia) in 2003, and received his PhD in 2006 from the same university and his DSc(Tech.) degree from the University of Oulu (Finland) in 2008. Currently, he is a docent in the University of Oulu. His scientific interests are in the area of nanobiophotonics, nanoparticle-light-tissue-cell interaction, including biotissue-mimicking phantoms, deep-tissue imaging using up-conversion nanoparticles, enhancement of skin UV protection by sunscreens, cell optoporation by plasmonic nanostructures.

Alexander V. Bykov is a postdoctoral researcher in the University of Oulu. He received his MSc diploma in physics at the M.V. Lomonosov Moscow State University in 2005 and his PhD in 2008 from the same university. In 2010, he received his DSc(Tech.) degree from the University of Oulu. His scientific interests are in the area of biophotonics, noninvasive optical diagnostics, theory of light propagation in scattering media including biotissues and numerical simulation of light transport.

Valery V. Tuchin is a professor and chairman of optics and biophotonics at Saratov State University, Russia. He is also the head of laboratory, Institute of Precision Mechanics and Control, RAS. His research interests include biophotonics, tissue optics, laser medicine, tissue optical clearing, and nanobiophotonics. He is a member of SPIE, OSA, and IEEE, and a fellow of SPIE and has been awarded Honored Science Worker of Russia, SPIE Educator Award, and FiDiPro (Finland).

Adam Cenian is the head of the Physical Aspects of Ecoenergy Department in the Szewalski IFFM, Polish Academy of Sciences in Gdask. He is specializing in laser technologies, plasma physics, and chemistry, as well as ecoenergy technologies, such as photovoltaics and bioenergy.